



Hydroclimate extremes in a north Australian drought reconstruction asymmetrically linked with Central Pacific Sea surface temperatures

K.J. Allen^{a,b,*}, M.B. Freund^c, J.G. Palmer^{b,d}, R. Simkin^e, L. Williams^f, M. Brookhouse^g, E.R. Cook^h, S. Stewartⁱ, P.J. Baker^a

^a School of Ecosystem and Forest Sciences, University of Melbourne, 500 Yarra Boulevard, Richmond 3121, Australia

^b The Australian Research Council Centre of Excellence for Biodiversity and Heritage, Australia

^c Agriculture and Food, CSIRO, Australia

^d School of Biological, Earth and Environmental Sciences, University of New South Wales, Sydney, NSW 2052, Australia

^e School of the Environment, Yale University, 195 Prospect St, New Haven, CT, 06511, USA

^f Department of Forest Resources, University of Minnesota, St Paul, MN 55108, USA

^g School of Biology, Australian National University, 134 Linnaeus Way, Acton ACT 2601, Australia

^h Lamont-Doherty Earth Observatory, Palisades, New York 10964, USA

ⁱ Land and Water, CSIRO, Sandy bay, Hobart 7005, Australia



ARTICLE INFO

Keywords:

Drought

Tree-rings

Standardised precipitation evaporation index

Monsoonal Australian north

Central Pacific

El Niño-Southern Oscillation

ABSTRACT

An understanding of tropical hydroclimate variability, the associated drivers and how it is likely to change is a major scientific and societal challenge that is acutely hampered by short instrumental records. We present a 246-year tree-ring drought reconstruction of the Standardised Precipitation Evaporation Index (SPEI) for monsoonal northern Australia for the end of the wet season (March–May; MAM). This reconstruction extends the instrumental record back by 150 years. Around one third of total annual rainfall falls during MAM, making it a crucial component of the monsoonal cycle. MAM is also the season most impacted by the differential decay process of Central Pacific (as opposed to Western Pacific) El Niño events that are linked with dry conditions over northern and northwestern Australia more generally. Our reconstruction therefore provides an opportunity to consider how central Pacific variability has modulated MAM hydroclimate in Australia's monsoonal north over the past two and a half centuries. We found that MAM hydroclimate extremes in the region have a strong, but asymmetric relationship with central Pacific sea surface temperatures (SSTs) and ENSO indices. Extremely wet MAMs in monsoonal north Australia were associated with cooler SSTs, above average rainfall across much of Australia, and often coincided with La Niña events. The spatial relationship between dry extremes and Pacific SSTs during dry events was generally, but weakly, consistent with the SST signature of central Pacific El Niño events. The association between reconstructed dry extremes in the monsoonal north and dry conditions across the rest of Australia is also less extensive and weaker than for wet events. Results suggest that more extreme wet events in the Australian monsoonal north likely reflect cool central Pacific SSTs and later termination of the Australian monsoon. Consecutive years with extremely dry MAMs became more frequent over the latter part of the 20th Century while the probability of an extreme dry MAM followed by an extreme wet MAM the next year peaked in the mid 20th Century and has since declined.

1. Introduction

At the global scale, relatively little is understood about high-resolution hydroclimate prior to instrumental records (Smerdon and PAGES Hydro 2k consortium, 2017) and uncertainty about future hydroclimate is high (Cook, 2019). Yet, variability in hydroclimate has

profound impacts on environments and human societies. Drought can contribute to the fall of major civilisations (Buckley et al., 2010; Goswami et al., 2019) and has been suggested as a factor in the recent Syrian crisis (Kelley et al., 2015). Multi-year droughts can drive ecosystem collapse (Godfree et al., 2019) and impose serious constraints on urban and agricultural water supplies. Pluvial events can drive

* Corresponding author.

E-mail address: Kathryn.Allen@unimelb.edu.au (K.J. Allen).

renewal of arid systems or pave the way for the rise of civilisations (e.g. Pederson et al., 2014), but major flood events can have devastating and costly consequences (Rojas et al., 2013).

As an important driver of hydroclimatic variability with near-global impacts, El Niño–Southern Oscillation (ENSO) is associated with widespread disasters such as drought and flood (Lesk et al., 2016) and has major impacts on tropical hydroclimate in particular. Over the past decade, there has been much discussion about the difference between the canonical, or eastern Pacific El Niño (EP) that has a peak signature in the eastern Pacific in the Southern Hemisphere spring, and the often less intense central Pacific El Niño (CP) events that exhibit a peak signature in the central Pacific. While CP El Niño events are less intense and evolve differently than EP El Niño events (Rensch, 2019; Zhang et al., 2015), they can still have significant impacts on global and regional precipitation patterns (Larkin and Harrison, 2005; Ashok et al., 2007; Hendon et al., 2009; Wang and Hendon, 2007; Kug et al., 2009; Zhang et al., 2015). These impacts and their geographical distribution differ from those of EP El Niño events. This diversity in ENSO expression contributes to limited confidence in projections of how ENSO is expected to change under climate warming scenarios (IPCC, 2019). Generally short (<100 years) instrumental records in tropical regions, asymmetries between the impacts of La Niña and El Niño events on hydroclimate, and the influence of different phases of the Interdecadal Pacific Oscillation (IPO; Power et al., 2006; King et al., 2013), further contribute to the complexity of the relationship between hydroclimate and ENSO.

Australian rainfall, including monsoonal rainfall occurring from October to April, is sensitive to the zonal distribution of sea surface temperature (SST) anomalies and therefore the diversity in ENSO events (Wang and Hendon, 2007). This sensitivity contributes to the complexity of climate processes affecting the Australian monsoon and its predictability (Moise et al., 2015; Taschetto et al., 2009). EP El Niño events have commonly been linked to spring rainfall deficiencies across much of eastern Australia (McBride and Nicholls, 1983; Taschetto and England, 2009 amongst others). In contrast, CP El Niño events are the leading mode of Australian rainfall in March–May (MAM) with a geographical footprint focused on the monsoonal north and northwest of Australia (Taschetto and England, 2009). These CP El Niño events also tend to lead to a more intense but shorter monsoon (Taschetto et al., 2009). La Niña events are typically associated with wet conditions and flooding in eastern and northern Australia (Risbey et al., 2009), and debate exists over whether or not distinctions between CP and EP La Niña events exist (e.g. Kug and Ham, 2011).

Scientific interest in the relationship between ENSO and Australian monsoonal rainfall has predominantly focused on the onset (~October to December) and core (~November–March) of the monsoon season (Nicholls et al., 1982; Hendon and Liebman, 1990; Drosdowsky, 1996; Kajikawa and Wang, 2010 amongst others) rather than the transition period from the wet to dry seasons (~March–May). High quality rainfall records for the region reveal that ~30% of annual rainfall (Sep–Aug water year) typically occurs in MAM, although this can be as high as 50% in some years and locations (updated records available from www.bom.gov.au). The intensity and timing of the wet-dry transition during MAM is also highly variable from year to year (Drosdowsky, 1996). Furthermore, easterly disturbances between April and June can extend the northern wet season (Southern 1966 in Taylor and Tulloch, 1985). As elsewhere, the lack of long hydroclimate records in the monsoonal Australian north hinders our understanding of monsoon dynamics over longer time frames, including changes in onset and retreat (Moise et al., 2015; Taschetto and England, 2009; Brown et al., 2016).

Longer records are necessary to better understand both the variability in monsoon precipitation patterns and their relationship with major drivers of climate variability such as ENSO. Here we present the first annually resolved drought reconstruction for the March–May (MAM) season in monsoonal northern Australia based on a local tree-ring network of *Callitris intratropica* (cypress pine). By relying solely on local proxy records, we avoid incorporating climate variability

information from other remote locations. A locally sourced record allows for a more locally relevant analysis of potential influences of major climate modes on hydroclimate. Previous use of remote proxy data was necessitated by the lack of reliable annually resolved proxy records in the region. The strong MAM moisture signal in the tree-ring chronologies (Allen et al., 2019; Fig. S1) makes sound physiological sense because precipitation in SON and MAM is less abundant than for the core of the wet season, and hence more limiting to growth (Fritts, 1976). This MAM signal therefore provides an exciting opportunity to assess the impact of CP ENSO events on the end of the Australian monsoon over the past two and half centuries in the region, and for a period of the year when the Indian Ocean Dipole (IOD), another important mode of tropical hydroclimate variability, is typically inactive (Risbey et al., 2009).

2. Materials and methods

2.1. Instrumental data used for the reconstruction

The Standardised Precipitation Evapotranspiration Index (SPEI; Vicente-Serrano et al., 2010) that measures drought and is based both on soil moisture and temperature was used for this study. It was obtained from the CRU data portal (CSIC: <https://digital.csic.es/handle/10261/153475>); each grid cell covers $0.5 \times 0.5^\circ$. Allen et al. (2019) demonstrated that the strongest links between drought indices (SPEI and self-calibrating Palmer Drought Severity Index; sc-PDSI) and *Callitris intratropica* ring widths in the monsoonal Australian north occur in the Austral spring (SON) and autumn (MAM) transitional seasons. This result holds for each of the chronologies used in this study and is most consistent for MAM (Fig. S1). Given that the relationship between drought and the chronologies rapidly decreases over the months of the ‘core’ wet season (Fig. S1), we used the SPEI rather than the sc-PDSI due to its scalability and the strong autocorrelative structure of the sc-PDSI. We have reconstructed the 3-month SPEI for MAM because the tree-ring drought relationship is consistently high for this season (Fig. S1). In all cases, we used gridded and instrumental data for the 1920–2006 period only. Although gridded data prior to 1920 does exist for the tropical north, it is based on relatively few observational records and hence less reliable.

2.2. The drought reconstructions

We used six tree-ring chronologies, based on seven sites, from the north Australian monsoon zone in our reconstruction (Fig. 1). Three of these have been previously published (PC; Baker et al., 2008; KOR and MUR; Allen et al., 2019). The remaining chronologies, TIW, MN, LIT and HAY, were recently developed based on material collected in 2007/08 (Fig. 1; Table 1). The close proximity of TIW and MUR combined with the former’s low sample depth and the latter’s end date in 1973 meant it made sense to combine these two data sets to produce a single chronology that was longer and of higher quality than either of the original two. A negative exponential or negatively sloped linear regression line was used to detrend data; there was clear evidence of this type of growth trend in the majority of series. The final chronologies were all developed in the signal-free framework (Melvin and Briffa, 2008) using a biweight mean.

A nested point-to-point principal component regression approach (PPR) was used to produce the reconstructions in this study. The same approach has been used to develop the various drought atlases based on the sc-PDSI (e.g. Cook et al., 2010; Palmer et al., 2015). Each successive nest is longer than the last but uses fewer chronologies. This nested approach acknowledges that the number of predictor chronologies decreases further back in time. Each nest is rescaled against the instrumental data after which nests are spliced together to produce the final reconstruction for each grid cell.

The reconstruction for an individual grid cell made use of information from all six final chronologies. We used an eight-weight (0, 0.1,

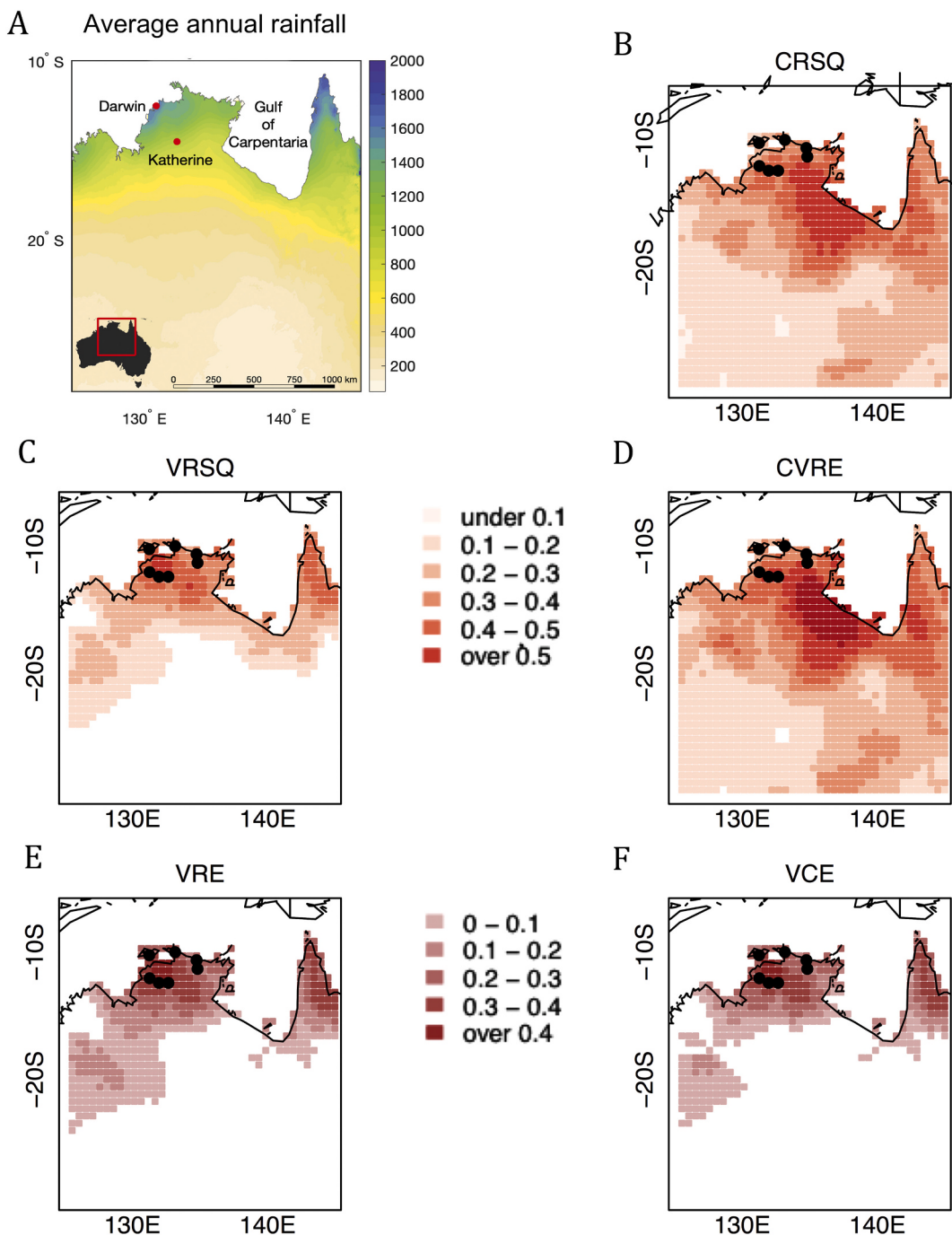


Fig. 1. A. Map showing area covered by gridded SPEI3 reconstructions. B–F Reconstruction statistics: Calibration R2 (B); verification period R2 (C); Cross validation RE (D); verification period RE (E); verification period coefficient of efficiency (F). All grid cells shown in colour have positive values. All reconstructions with VRE > 0 (423 of 1179) were used for the PCA.

Table 1
Location and length of *Callitris intratropica* sites used in reconstructions.

Chronology	Longitude	Latitude	Period	Number of dated series in chronology
KOR	134.32	-12.65	1761–2015	165
MUR	132.70	-11.5	1845–1973	69
TIWI	130.83	-11.71	1877–2007	21
LIT	130.85	-13.29	1862–2007	57
HAY	131.53	-13.60	1897–2006	22
PC	132.21	-13.61	1847–2006	30
MAN	134.25	-12.05	1870–2007	52

0.25, 0.5, 0.67, 1.0, 1.5, 2) scheme to produce eight different drought reconstructions for each grid point. Weights were applied to each predictor chronology based on its correlation with the target grid point SPEI over the calibration period (1961–2006). Similar weighting regimes have been used elsewhere (e.g. Cook et al., 2010; Palmer et al., 2015) to produce a final ensemble reconstruction for each grid point. For each reconstruction in this study, the predictors and predictands were autoregressively modeled to ameliorate differences in the autocorrelative structure of the tree ring and climate data sets. The eight resultant reconstructions for each grid point were then averaged to produce a final reconstruction for each grid point. This final model for each grid point, based on the 1961–2006 calibration period, was then tested against

instrumental data for the period 1920–1960 that was withheld from model calibration.

We deliberately chose a large area ($125\text{--}143^{\circ}\text{E}$, $10\text{--}29^{\circ}\text{S}$) for our reconstructions because this would help identify any distinctive geographic pattern in the area over which the reconstructions demonstrated skill. A suite of commonly used calibration (R^2 for the calibration period (CRSQ); cross-validation reduction of error (CVRE)) and verification statistics (R^2 for the verification period (VRSQ); reduction of error for the verification period (VRE); coefficient of efficiency for the verification period (VCE)) across the region help to define the spatial expanse over which the current collection of sites can be used to detect the influence of regional drought, and help guide future site selection. For further detail on these statistics see Cook et al. (1999).

We examined the first PC of the field reconstruction to assess the common temporal variability of drought, but only for those grid points with a $VRE > 0$ (423 grid points of 1179). We did not use the full set of available reconstructions across the broader area in the PCA because this would introduce undesirable noise from very low quality reconstructions into the subsequent analyses. By including only these grid cells with a $VRE > 0$, our analyses focus on the Köppen-defined monsoon zone in Australia (Fig. 1). This first mode of these 423 reconstructions was used in all subsequent analyses (see Fig. 1 for area this covers).

2.3. Identifying consecutive extremes and swings from one extreme to the other

Information on changes in the frequency of swings from an extreme wet (dry) event to an extreme dry (extreme wet) event, and in the number of consecutive extreme wet (dry) MAMs over the period of our reconstruction, can provide valuable context for any such changes in recent decades. Therefore, we examined our reconstruction for both consecutive wet (dry) extremes and swings between wet and dry extremes.

We used three sets of thresholds to define increasingly extreme dry and wet events in both the instrumental data and PC1 of the reconstruction. This defined three sets of composites. The first and least extreme (termed ‘moderate’ extremes) of these composites was defined by the thresholds that identified the upper (UT) and lower (LT) terciles of SPEI values in the 1920–2006 period for each of the reconstruction and instrumental data in turn (upper and lower terciles each contained 28 years). Increasingly extreme wet (dry) extremes composites were defined by thresholds for the upper and lower ten (U10 and L10) events (i.e. $n = 10$ in each of these composites). The most extreme event composites were defined by the thresholds for the upper and lower five (U5 and L5) events in the 1920–2006 period ($n = 5$ in these composites). The thresholds for the reconstruction composites defined in the above manner were: -1.83σ , -1.49σ , -0.39σ , 0.43σ , 1.06σ and 1.39σ (from L5 to U5). For the instrumental data, thresholds were: -1.76σ , -1.41σ , -0.41σ , -0.67σ , 1.26σ and 1.67σ (from L5 to U5).

These thresholds were then applied to the leading mode of the entire reconstruction to identify moderately extreme, extreme, and very extreme wet and dry events for the past 246 years. This then allowed us to estimate the empirical probability of swinging from a wet (dry) extreme to dry (wet) extreme MAMs using a 30-year sliding window. It also allowed us to identify multi-year wet or dry MAM extremes based on a count of consecutive years with events more extreme than each of the respective thresholds.

2.4. Relationship between drought reconstructions, precipitation and the Pacific Ocean

The impact of more extreme drought and pluvial events can be significant and as climate changes, improved knowledge of how extremes have changed in the past is increasingly important. As MAM drought/pluvial conditions in the Australian tropical north have previously been linked with the Pacific Ocean (Cai and Cowan, 2009; Taschetto and

England, 2009; Taschetto et al., 2009), we examined the relationships between extreme hydroclimate events in our MAM SPEI3 reconstruction over the 1920–2006 period and both Pacific sea surface temperatures (SSTs) and precipitation. We also undertook the same comparison with the UT/LT, U10/L10 and U5/L5 composites in the instrumental data. We used the monthly observed sea surface temperature dataset HadISST (Rayner et al., 2003; <http://www.metoce.gov.uk/hadobs/hadisst/>) and the global, monthly precipitation dataset GPCC Full Data Reanalysis v.7 Version (Becker et al., 2013). We also compared outgoing longwave radiation with the composites, this provides an independent check on the results of our comparison of the composites with SSTs. For example, negative OLR anomalies (more convection) over a region would be consistent with warm SSTs and wetter conditions. Satellite-based (OLR) observations used here are based on the NOAA Interpolated OLR dataset (Lieberman and Smith, 1996).

To see if there were discernible links with El Niño or La Niña events, we also compared the extremes composites (instrumental and reconstruction) with a number of reference series of El Niño and La Niña events. Each reference set contains a slightly different list of El Niño and La Niña events. These reference series included events listed on the Australian Bureau of Meteorology website (www.bom.gov.au), the Meyers et al. (2007) compilation, and a recently published list based on the seasonal evolution of El Niño events (Freund et al., 2019) that distinguishes between CP and EP events. We did not attempt to distinguish between CP and EP La Niña events given ongoing debate about whether or not it is appropriate - or possible - to distinguish between CP and EP La Niñas (Cai and Cowan, 2009; Kug and Ham, 2011; Zhang et al., 2015; Song et al., 2017) when cold anomalies during La Niña events are typically displaced further west than is the case for El Niño (Hendon et al., 2009).

Bootstrapping procedures were used to assess whether SST and precipitation anomalies, or the number of El Niño/La Niña events, were significantly above or below average in the years included in each of the extremes composites (i.e., UT/LT, U10/L10, U5, L5). In the case of the SST and precipitation data, all possible samples of the same length (number of years) as the each of the composites were generated for each grid point, providing a distribution against which the SST and precipitation anomalies could be tested for significance. For example, average SSTs/precipitation in UT and LT years were compared with mean SST/precipitation in all the bootstrapped samples randomly selected from the 1920–2006 period, each sample of which was 28 years in length. Where average SST or precipitation values for the extremes composite year sets exceeded 95% of the SST/precipitation bootstrapped averages, the result was deemed significant. Essentially the same procedure was applied to the ENSO reference series. In this case, however, the actual number of El Niño and La Niña events (as defined by the various reference series) in the UT/LT, U10/L10 and U5/L5 composites were compared against the bootstrapped distributions of the numbers of El Niño and La Niña events.

The OLR data series began only in 1948, so no attempt was made to assess significance of departures from the mean. We simply computed the anomalies at each grid point for the years in each of the extremes composites.

3. Results and discussion

3.1. The drought reconstruction

Basic reconstruction calibration and verification statistics show that the spatial extent of reconstruction skill (VRE , $VCE > 0$) of this small network of sites extends from the central west to the most northern part of the domain where average annual rainfall exceeds 1600 mm (Fig. 1; VRE , VCE). Both calibration and verification period correlations (CRSQ; VRSQ) with the SPEI-3 are strongest in the northern part of the domain, with peak strength of CRSQ occurring in the southwest corner of the Gulf of Carpentaria (Fig. 1). The pattern of CVRE is similar to that for CRSQ,

although stronger results are evident for a smaller region around the southwest corner of the Gulf of Carpentaria. Perhaps unsurprisingly, strongest verification (VRE, VCE) occurs in the north-northwest of the domain that is proximate to the tree-ring sites.

The first principal component of the 423 MAM reconstructions with $VRE > 0$ accounts for $\sim 84\%$ of the variance. The average CRSQ for these 423 reconstructions used in the PCA was 33.4%. The first principal component of the reconstructions closely tracks PC1 of the gridded SPEI-3 data that accounts for only $\sim 54\%$ of the variance (Fig. 2). The considerably higher level of variance accounted for in the first empirical orthogonal function of the reconstructions is likely due to reliance of all reconstructions across the domain on the six geographically clustered chronologies (Fig. 1). In contrast, the gridded SPEI data does not depend

solely on information in the north-northwestern corner of the domain. Opposing trends in MAM precipitation and drought intensity in the monsoonal northwest (increased precipitation) and northeastern Queensland (decreased precipitation) since the 1980s (Gallant et al., 2013; Moise et al., 2015) may partly account for these differences in variance explained by PC1 of the reconstructions and PC1 of the instrumental SPEI data.

A number of multi-year dry and wet periods are evident in the PC1 of the reconstruction (Fig. 2A). These multi-year wet and dry periods described in this section are not based on the thresholds for the composites described above. Rather, in this section, we define a multi-year dry/wet event as one for which all years were at least 0.5σ below/above the mean and at least two years were $\geq 1\sigma$ below/above the mean.

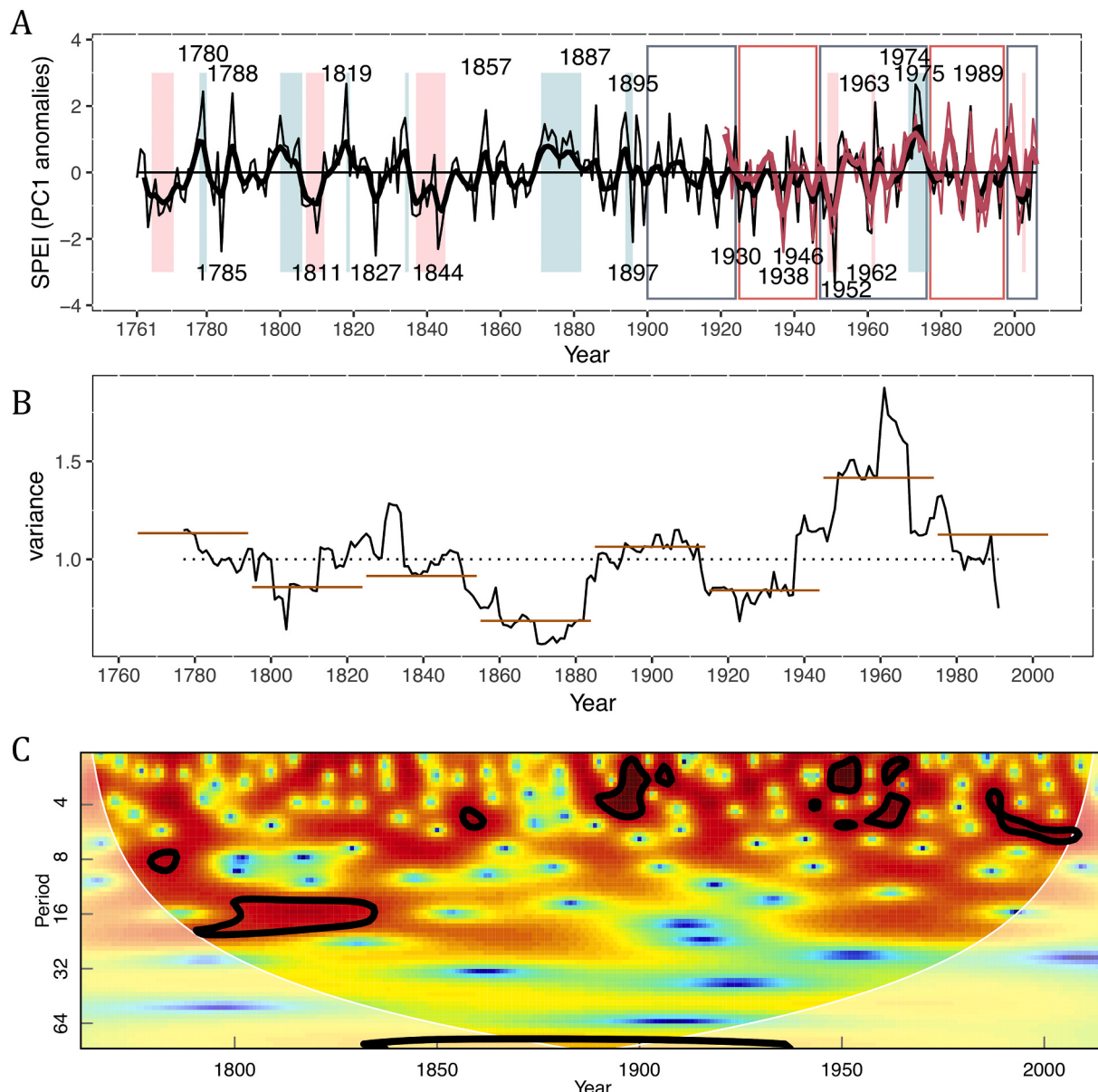


Fig. 2. A. PC1 of ensemble reconstruction (black; $\sim 84\%$ of variance) and PC1 of gridded SPEI data for same region (red; 54% of the variance). Pink bands represent generally dry periods (a continuous period that includes at least two years more than one standard deviation below the mean and where all years are at least 0.5σ below the mean) while blue bands represent generally wetter periods (a continuous period that includes at least two years more than one standard deviation below the mean and where all years are at least 0.5σ above the mean). The outlined periods show negative (blue) and positive (red) IPO periods. The 10 lowest and highest reconstructed SPEI values are noted on the plot. Thick lines are 5-year Gaussian smooths. B. Variance of reconstruction based on 30-year running windows (black) and consecutive non-overlapping 30-year periods (red). C. Wavelet of the reconstruction showing stronger variability ~ 16 years in the earlier part of the reconstruction but stronger high frequency variability after ~ 1900 . (For interpretation of the references to colour in this figure legend, the reader is referred to the web version of this article.)

The reconstruction suggests that, generally, high SPEI value periods (wet) occurred for 1801–06, 1818–19, 1834–5, 1871–82, 1894–6 and 1971–7, and low SPEI value periods (dry) occurred for 1765–75, 1807–12, 1837–46 and 1942–52, 1961–2 and 2002–03 (Fig. 2A). The worst drought year was 1952, towards the end of a relatively dry period. This year was noted as a record drought year in the Katherine region, with perennial grasses in native pasture dying across the region (Taylor and Tulloch, 1985). Interestingly, the pattern of monthly precipitation for this year (1951–2 was an El Niño year: Bureau of Meteorology) was consistent with that of many years over the 1870–1985 period (Taylor and Tulloch, 1985). The single wettest year in the reconstruction was 1820. It was closely followed by 1974, which coincided with the filling of Kati Thanda–Lake Eyre and major flood events in eastern Australia. There was a hiatus in very wet events (top 10 in the overall reconstruction; Fig. 2A) in the first half of the 20th Century during which five of the top 10 driest events occurred. This period was immediately followed by a 25-year period in which four of the top 10 wettest events in the record occurred. The remaining top 10 dry events occurred over the 65-year period from 1780 to 1845. The largest variance in the reconstruction occurred in the middle of the 20th Century with less variability occurring around 1800, in the late 1800s, and again from ~1920–40 (Fig. 2B&C). These dips in variability are consistent with those in Javanese streamflow (D'Arrigo et al., 2011) and known periods of lower ENSO variability that have been attributed to changes in the 4–7 year frequency band (Allan, 2000). Our drought reconstruction, however, indicates that variability in this band has been strongest since the late 1800s (Fig. 2A, C). In contrast, medium frequency variability (~16-year) in the reconstruction persists from ~1800 to ~1880 (Fig. 2A) and is weakest from ~1900–1950 (Fig. 2C). Reduced decadal-scale variability in the Li et al. (2013) ENSO reconstruction in the 20th Century and decadal-scale variability in coral records in the late 1800s (Li et al., 2013) are consistent with our results. Moderate associations with other reconstructions of Pacific SSTs and hydroclimate reconstructions for the region are discussed in the Supplementary material (Figs. S2 & S3).

3.2. Consecutive extreme dry/wet MAMs and swings from one extreme state to the other

Consecutive years of drought or pluvial conditions can have significant impacts on the environment and economy, especially in the Australian tropics where ecological processes are highly dependent on the annual hydroclimate cycle (Warfe et al., 2011). For example, consecutive La Niña events that result in wetting replenish water resources, with implications for agricultural enterprises in the region. Similarly, changes from a very wet (dry) to a very dry (wet) state, can also have significant impacts on landscapes and environments.

Where rainfall variability is linked to ENSO variability, as it is much of the tropics, modelling indicates that the risk of major rainfall disruptions increases (medium confidence) and that more frequent swings from one extreme ENSO state to the other are expected as the climate warms (IPCC, 2019). Whereas most EP El Niño events are followed by La Niña conditions, weak or moderate CP El Niño events are less likely to be followed by La Niña conditions (Kug et al., 2009) and are more persistent (Allan et al., 2019). The 2014/15 CP El Niño is one example of this; it was followed by a strong EP El Niño year in 2015/16, resulting in two consecutive dry years.

Although we can discuss only MAM and not the core of the wet season or what happens in the dry season, it is still very relevant to consider consecutive wet (dry) MAMs that are extreme in nature. This is because particular ecological processes occur in this season, for example, native bees make sugarbag, MAM is mating season for a variety of species, burning of the landscape by indigenous peoples occurs at this time and particular foods become available at this time (e.g. see Indigenous weather knowledge at <http://www.bom.gov.au/iwk/>; Redhead, 1979; Cook and Heerdegen, 2001; Vardon et al., 2001; Woinarski and Mackey, 2007). Therefore, consideration of changes in the frequency of

swings from one extreme state to another or the occurrence of consecutive dry (wet) MAM extremes over time may assist with understanding past variability in resource availability and ecological function. Such understanding has implications for modelling the future impacts of changes in persistence of wet (dry) MAMs on ecological process.

In what follows we discuss what PC1 of our reconstruction suggests about consecutive wet (dry) extremes and what it suggests about swings from one extreme state to the other. We refer to the extremes composites described in the Methods (i.e., UT/LT, U10/L10, U5/L5).

3.2.1. Consecutive year MAM extremes

There are similar numbers of multi-year (two or more years) wet (UT) and dry (LT) extreme events that occur throughout the reconstruction (Fig. 3A). There is, however, a hiatus in reconstructed extremes that extends from the end of the 1800s until ~1950 that also coincides with a shorter hiatus in cool SSTs (~1920–1950; Fig. S4). The longest multi-year wet extremes (UT) are: 1798–1803 (6 years), 1871–1876 (6) 1877–1881 (5), 1953–1956 (4) and 1971–1977 (7). The longest multi-year dry extremes (LT) in the reconstruction include: 1768–1772 (5), 1807–1812 (6), 1949–1952 (4) and 2001–2004 (4). The first of these must be regarded with caution due to the low number of samples included during this period of the reconstruction. There is a tendency for multi-year wet extremes (UT) to be more persistent than multi-year extreme dry events (LT), and this is consistent with duration of the cool and warm phases of ENSO respectively. Overall, there is no obvious change in the frequency of multi-year wet extremes (UT), although it does appear that the frequency of multi-year dry extremes (LT) may have increased (Fig. 3A).

Extreme and very extreme (U10 & U5) multi-year wet events are more frequent than extreme and very extreme multi-year dry events (L10 & L5; Fig. 3A). As might be expected, the number of years for which these more extreme MAM conditions persist is less than is the case for persistent UT/LT MAMs. There are only two instances of very extreme wet multi-year events (U5), and none of very extreme (L5) multi-year dry events.

The approximately equal numbers of multi-year moderately extreme wet and dry events (UT and LT) does not appear consistent with previous work. Both Allan et al., 2019 (Niño4 reconstruction) and Cook (unpublished Niño3.4 reconstruction) found a greater number of multi-year cool SST (likely to be wet years) than warm SST events (likely to be dry events) (Fig. S4). However, the greater number of U10/U5 wet extremes than L10/L5 (dry) extremes is consistent with both Allan et al. (2019) and the Cook Niño3.4 reconstruction (Fig. S4).

3.2.2. Swings between wet and dry MAMs

Based on running 30-year periods, the probability of swinging from one extreme state to another increased for moderately extreme events (LT to UT in particular) after ~1900 (Fig. 3B). No swings between more extreme states (U10/L10 and U5/L5) occurred prior to 1897, and the most extreme swing - an L5 to an U5 event - occurred in 1897–98. The increased tendency to swing from one moderately extreme state in MAM to the other (i.e. from UT to LT or LT to UT) in the early to mid 20th Century (Fig. 3B) is consistent with expectations outlined in the IPCC (2019). However, the prolonged negative phase of the IPO from ~the mid 1940s to the mid 1970s may also have played a role in there being a greater number of swings in the mid 20th Century (cf. King et al., 2013).

Both the decrease in swings from dry to wet events since ~1950 and the apparent increase in multi-year dry events since this time are consistent with an observed increase in the number of CP events relative to the number of EP El Niño events since ~1950 (Freund et al., 2019). If the apparent trend towards more frequent multi-year dry MAMs continues (Fig. 3B) - and this trend is indeed unprecedented over long time frames - it has the potential to impair ecosystem functioning going forward, and have significant implications for indigenous peoples and land managers who both rely on the environment for subsistence, enterprise and cultural purposes. Similarly, if IPO phase modulates the frequency

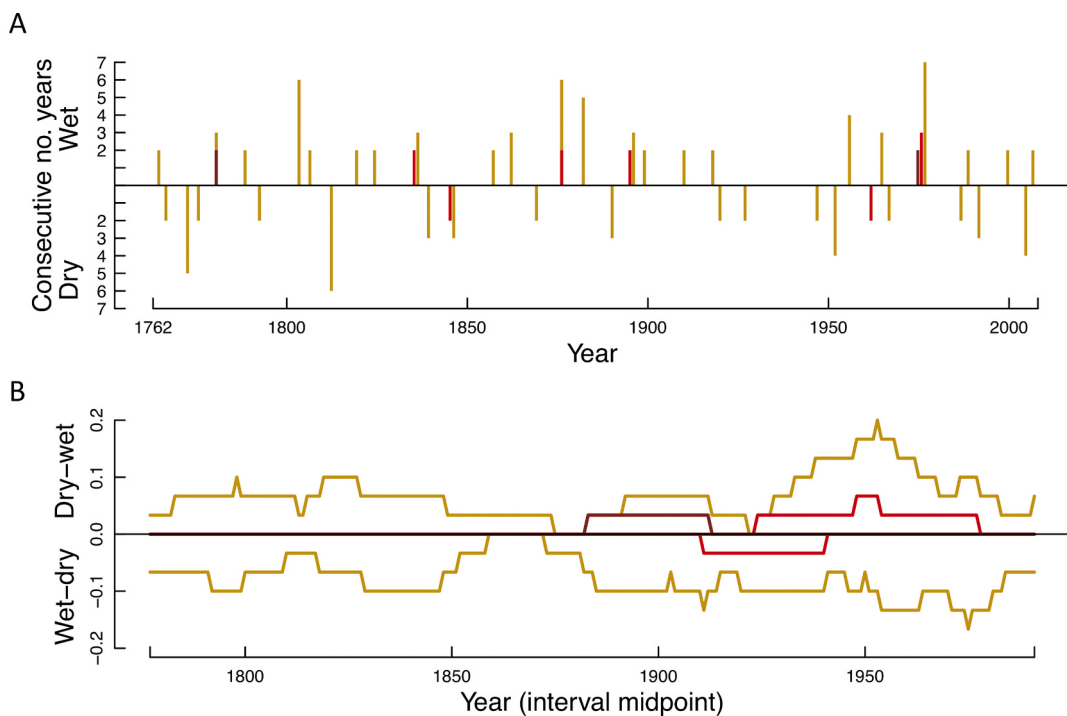


Fig. 3. A. Length of consecutive wet and dry autumns in the reconstruction based on the six composites (UT/LT, U10/L10, U5, L5). Length of bars represents the number of successive dry autumns. B. Changes in the probability (transition probability) of swinging from a more extreme wet (dry) event to a more extreme dry (wet event), based on 30-year windows. Golden brown represents (UT/LT), red (U10/L10) and dark red (U5/L5). See Fig. S4 for comparison of multi-year dry (wet) events in reconstruction with warm (cool) reconstructed SSTs. (For interpretation of the references to colour in this figure legend, the reader is referred to the web version of this article.)

of swings, and perhaps also extended dry (wet) periods, longer high-resolution records of both hydroclimate variability and ecosystem changes for the region, ideally for multiple seasons, will be required to improve our understanding of ecosystem impacts.

3.3. Drought, precipitation and Pacific Ocean sea surface temperatures

A somewhat asymmetrical relationship between the wet and dry extremes and both SSTs and the ENSO events is apparent in our results. For extreme wet MAM events in the monsoon zone (UT through to U5), results are relatively straight-forward: cooler Central Pacific SSTs yielded more extreme pluvial events across much of Australia (Figs. 4A, C, E, 5). For UT and U10 in particular, the co-occurrence of wet extremes and El Niño events was lower than expected (in the outlier range of the box and whisker plots) while the co-occurrence of wet extremes and La Niña events was significantly greater than expected. This pattern is stronger for the reconstruction than the instrumentally based SPEI-3 (Fig. 4). Interestingly, there was little difference in the co-occurrence of CP and EP El Niño events and extreme wet MAMs, although both were somewhat below the range of what might be expected (Fig. 4). Therefore, our results in Fig. 4 show very little support for a difference in the impact of CP and EP El Niño events on the MAM hydroclimate in monsoonal Australia. This is despite the fact that CP El Niño events are associated with a markedly shorter, but more intense, monsoon season, making high rainfall extremes during MAM less likely (Taschetto and England, 2009).

The association between the extremes composites and the La Niña indices (Fig. 4) are strongly consistent with the association of the wet extremes composites with significantly cooler Pacific SSTs (Fig. 5; instrumental, Fig. S5). Typically, the association between wet extremes (UT, U10, U5) and with cooler SSTs becomes stronger as the wet events become more extreme (from UT to U5; Fig. 5). Negative OLR anomalies over northern Australia indicate anomalously high convection, this

being consistent with the reconstructed wetter extremes in the region that occur at the same time as cool central Pacific SSTs (Fig. 5). The opposite occurs for dry extremes (Fig. 5). Although the spatial OLR patterns do not perfectly match those of SSTs across the entire Pacific Ocean, there is considerable similarity. The different lengths of the datasets as well as the different methodologies applied respectively to extract the SST and OLR patterns in relation to the extremes composites are likely a major reason for the observed differences.

The extent of the association between more extreme MAM pluvial conditions in the monsoonal north and precipitation over the Australian mainland also closely resembles the pattern shown by Cai and Cowan (2009). The spatial extent of significantly above average rainfall increases with increasingly wetter extremes in the monsoonal north and increasingly cooler Pacific SSTs (Fig. 5). Therefore, more extreme wet events in our reconstruction (1780, 1788, 1819, 1857, 1887, 1895; see Fig. 2) are most likely associated with a cool central Pacific and serve as an indicator for relatively strong La Niña events. Five of these six wet events coincide with the Freund et al. (2019) cool NCT index. Five coincide with cool events in both the Li et al. (2013) and Cook Niño3.4 series (data not shown).

The association between SSTs, dry extremes and El Niño events is less clear, however, demonstrating the asymmetrical nature of the relationship. There is a tendency for more extreme dry MAMs to co-occur with El Niño events, and to not occur at the same time as La Niña events. Although a greater number of dry events occur with CP El Niño events, when compared against the distribution of bootstrapped samples for either CP or EP (Fig. 4), it is apparent that this result is not significant. Similarly, the association between central Pacific SSTs and extreme dry events (LT, L10, L5) is less pronounced than for wet events (UT, U10, U5), with the strongest associations in the Coral Sea to the east of the Australian mainland (L5; Fig. 5; S5). Nevertheless, the actual spatial pattern of association with SSTs is strongly reminiscent of CP El Niño (Fig. 5; Ashok et al., 2007). The spatial pattern of reduced rainfall across

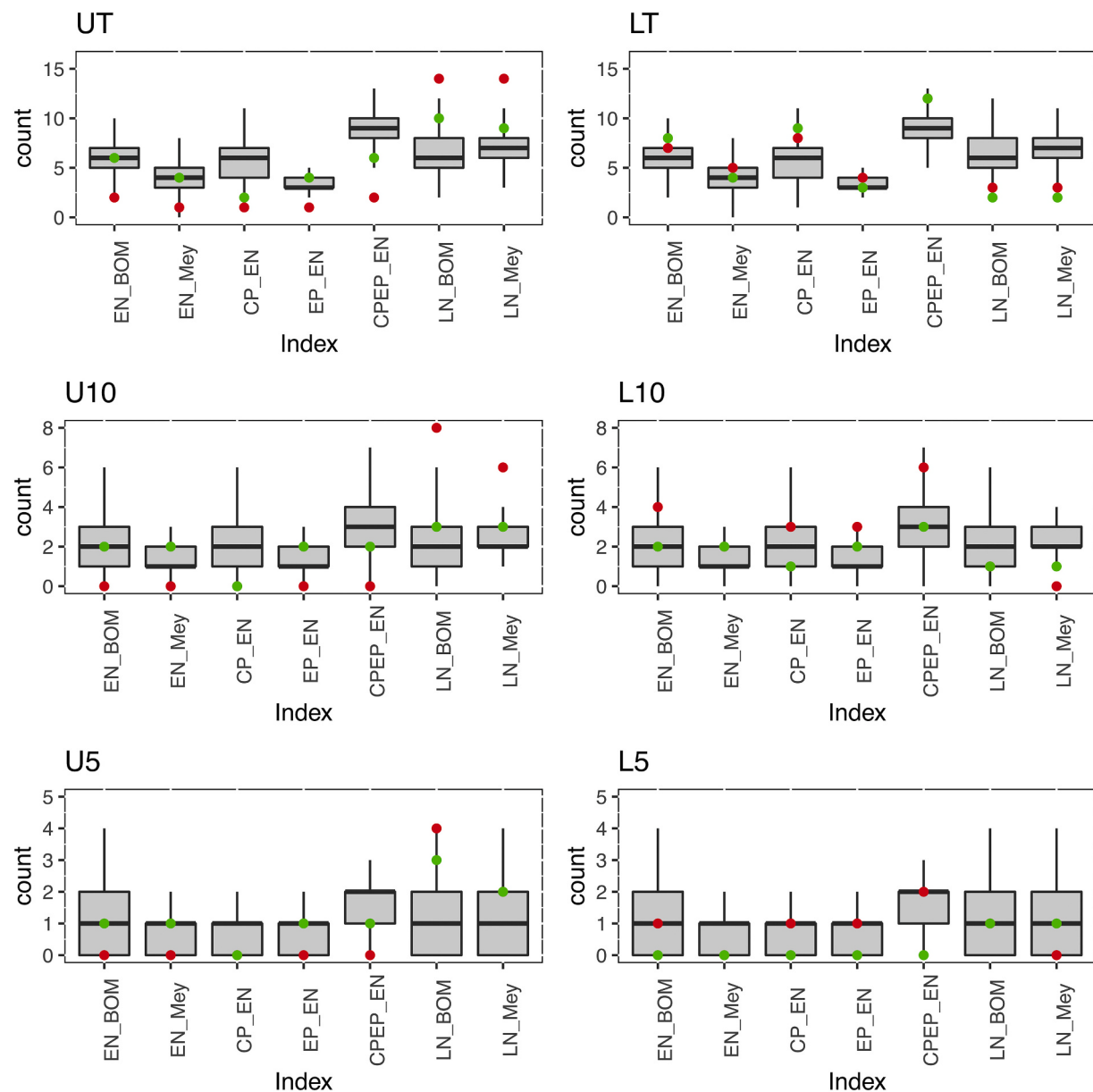


Fig. 4. Box plots comparing the co-occurrence of extremes in the various composites (UT/LT, U10/L10, U5/L5) and El Niño/La Niña events in various indices against that for the bootstrapped distributions. The various ENSO indices are listed along the x-axis. EN refers to El Niño and LN to La Niña. BOM refers to online data from the Australian Bureau of Meteorology (<http://www.bom.gov.au/climate/enso/enlist/>); Mey is the Meyers et al. (2007) classification; the CP and EP lists were developed by Freund et al. (2019); and CPEP refers to the combined list of CP and EP events by Freund et al. (2019). Red dots represent reconstructed data and green dots, the instrumentally based SPEI. (For interpretation of the references to colour in this figure legend, the reader is referred to the web version of this article.)

the Australian continent for the more extreme dry events (LT, L10 and L5) in the north is also consistent with the impact of CP El Niño events on MAM precipitation in northern and northwestern Australia as shown for instrumental data (Taschetto and England, 2009). In contrast to wet extremes, though, the area of significantly below average precipitation shrinks to include only the Australian monsoonal north as the drought becomes more extreme (Fig. 5).

That dry events appear more complex than wet events is perhaps not surprising due to the known asymmetrical relationship between the state of the Pacific Ocean and Australian rainfall (Power et al., 2006; King et al., 2013) whereby the magnitude of La Niña events has a greater impact than the magnitude of El Niño events. Our results for dry extremes may also reflect the influence of other factors, such as modulation by the Madden-Julian Oscillation (Ghelani et al., 2017). We have not differentiated between EP and CP La Niña events here, but Cai and

Cowan (2009) have noted that the five wettest MAMs since 1951 all coincide with a negative El Niño Modoki Index (EMI) while only one of the five driest MAMs coincides with a positive EMI. Although our results appear to contradict some previous work suggesting that Pacific SSTs do not affect hydroclimate in MAM in the monsoonal north, this difference could be attributable to the use of different definitions of the wet, dry and transition seasons amongst studies (e.g. Cook and Heerdegen, 2001; Drosdowsky, 1996; Evans et al., 2014).

3.4. Predictability

At the local level, MAM in monsoonal north Australia is a key period both for indigenous peoples and ecological processes (Warfe et al., 2011 and references therein; www.bom.gov.au/iwk/), and it is also relevant for agricultural enterprises (Yeates and Abrecht, 1996). Although the

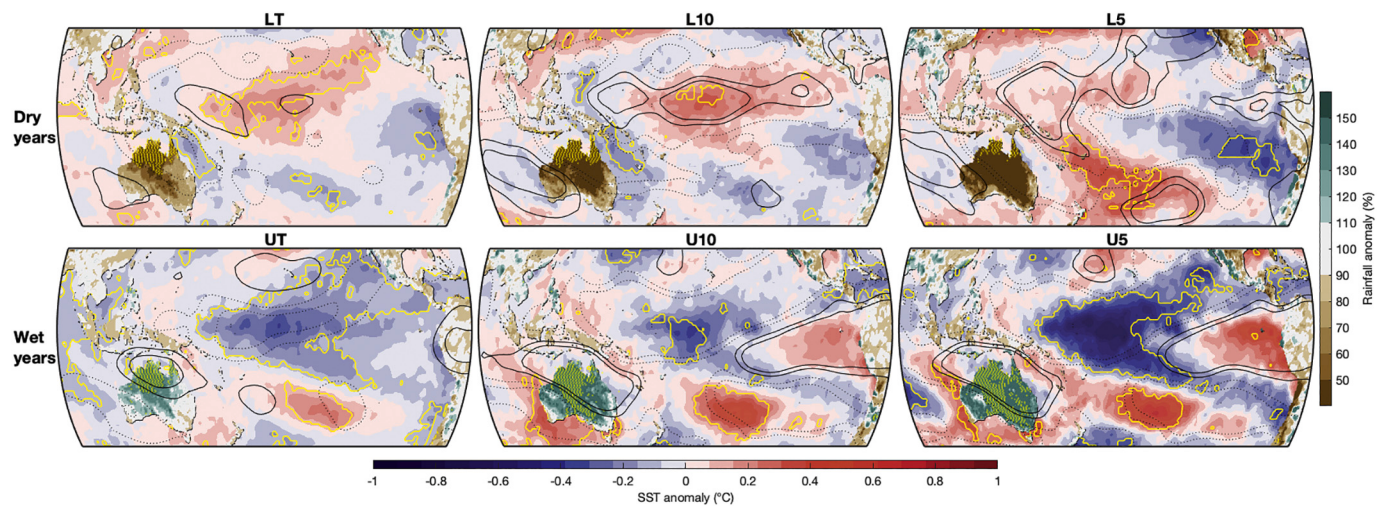


Fig. 5. Association between each of the extremes composites with Pacific SSTs and precipitation (land-only). Areas outlined in yellow had significantly higher/lower SSTs for years in the respective composites than 95% of the bootstrapped samples. Land areas with yellow dots indicate grid locations where precipitation for years in the respective composites were significantly higher or lower than average, again based on the bootstrapped samples. Solid black contours indicate greater convection (negative OLR anomalies); dotted lines show areas of less convection (positive OLR anomalies). Anomaly intervals are $\pm 5 \text{ Wm}^2$ and $\pm 10 \text{ Wm}^2$. OLR patterns are consistent with those shown for SSTs, with positive OLR anomalies occurring over northern Australia during dry periods. (For interpretation of the references to colour in this figure legend, the reader is referred to the web version of this article.)

strongest association between our reconstruction and each of SSTs and precipitation occur for MAM, this association – especially for more extreme wet events - becomes established during the prior spring and summer months (Fig. S6). Hendon et al. (2009) have previously commented on the ability to predict a CP El Niño event (for the summer season) one season in advance, potentially enhancing hydroclimate predictability in northern Australia. Similarly, Zhang et al. (2016) found that atmospheric and ocean conditions in the spring and early summer provide some predictive skill for dry season precipitation in Indonesia, especially for strong events. MAM precipitation across the maritime continent is also strongly associated with ENSO (Zhang et al., 2016), again highlighting the value of MAM hydroclimate reconstructions.

Corroborating evidence for our finding that extreme wet events in our reconstruction are likely associated with La Niña events would provide further evidence that the paleoclimate data provide a useful extension of the record of Pacific SST conditions. This would support incorporation of the data into modelling predictability of extended wet seasons in northern Australia. Persistence of dry conditions (Fig. 3A) may also provide evidence for CP El Niño conditions, while an increased frequency in swings from dry to wet conditions (Fig. 3B) may suggest a predominance of EP El Niño events. However, further work would be required before any use of our suggestive - but far from definitive - results were to be made. One avenue for further work in this area may be to make use of a new index recently developed by Williams and Patricola (2018) that succinctly characterises ENSO flavours based on the longitude of deep convection.

3.5. Improving the drought signal of the reconstructions

While our findings are significant in themselves, a much-extended network of *C. intratropica* will likely strengthen inference that can be derived from a spatial drought reconstruction in the tropics. An examination of the variously weighted reconstructions indicates that nests with a higher number of chronologies produced stronger statistics, especially for the verification period (Fig. S7). This indicates that more sites in the region are likely to improve reconstruction quality. O'Donnell et al. (2018) also found that the areal extent of the relationships between drought (as measured by the sc-PDSI in that case) and single sites of *Callitris columellaris* in the Pilbara and southwestern Western Australia was spatially limited. Additional sites further east may also

offer a longer-term perspective on seasonal differences between the monsoonal northwest and northeast of Australia (Moise et al., 2015). Although we focused our drought reconstruction on the MAM season, robust reconstructions of other hydroclimate variables such as rainfall or streamflow for other seasons such as SON may provide vital and complementary information.

4. Conclusions

There is only medium confidence in projections of ENSO and its impacts under climate warming (IPCC, 2019). Additionally, despite the importance of the end of the wet season (MAM), much greater attention has been paid to reasons for the variability in monsoon onset, long known to be associated with ENSO. Our drought reconstructions provide the first high-resolution extension (~ 150 years) of climate information regarding MAM in monsoonal Australia. The primary mode of the reconstruction demonstrates a clear connection with central Pacific SSTs and a broader relationship with MAM precipitation over much of the Australian mainland. The asymmetry in the relationship between hydroclimate in the monsoonal north and Pacific SSTs is consistent with previous instrumental-based studies: while increasingly extreme wet events are associated with increasingly cooler SSTs, dry extremes are more complex and likely also influenced by other factors. Nevertheless, the MAM precipitation signal across Australia, as well as the pattern of association with Pacific SSTs is highly suggestive of a CP El Niño influence. Swings from moderately extreme MAM wet events (UT) to moderately extreme dry MAM events (LT) increased in the early to mid 20th Century; but decreased towards the end of the century. This, and the apparent tendency towards more prolonged dry states when dry states do occur are consistent with expectations. These findings demonstrate the value of reconstructions of MAM hydroclimate in the monsoon zone, pointing to the importance of enriching the network of high-resolution palaeo-records for this region.

Contributions

KA conceptualised the study, led the formal analyses, investigation and writing. She was partly responsible for data curation. MF undertook formal analysis of the relationship between SSTs and the reconstruction. JP, RS, LW, MB, SS and PJB all assisted with data curation and

investigation. PB, JP and EC acquired funding for the project and PB provided overall project supervision. All authors assisted with writing, review and editing of the manuscript.

Data availability

Tree-ring data used in this study are available from the International Tree-ring Data-bank (<https://www.ncdc.noaa.gov/data-access/paleoclimatology-data/datasets>). They can also be provided by the corresponding author.

Declaration of Competing Interest

The authors declare no conflicting interests.

Acknowledgments

Work by KJA, LW and RS on this study was supported by Australian Research Council Discovery Project DP087874 to PB. We thank S Nichols, B French, B Dahl and D Norrie, L Prior and D Bowman for fieldwork, sample preparation and measurement of many samples in the MUR and KOR chronologies. Roseanne D'Arrigo provided her warm pool and Java PDSI reconstructions for comparison purposes. James Risbey provided constructive comments on analyses in this manuscript, and we thank Didier Monselesan and Carly Tozer for stimulating and informative discussions about the role of the MJO. We also thank two anonymous reviewers for their input that has helped improve this manuscript. Lamont-Doherty Earth Observatory contribution #8446. # 3# #8446.

Appendix A. Supplementary data

Supplementary data to this article can be found online at <https://doi.org/10.1016/j.gloplacha.2020.103329>.

References

- Allan, R.J., 2000. ENSO and climate variability in the last 150 years. In: Diaz, H.F., Markgraf, V. (Eds.), El Niño and the Southern Oscillation: Multiscale Variability and its Impacts on Natural Ecosystems and Society. Cambridge University Press, Cambridge, UK, pp. 3–56.
- Allan, R.J., Gergis, J., D'Arrigo, R.D., 2019. Placing the AD 2014–2016 ‘Protracted’ El Niño episode into a long-term context. The Holocene 1–16. <https://doi.org/10.1177/0959683619875788>.
- Allen, K.J., Brookhouse, M., French, B.J., Nichols, S.C., Norrie, D., Prior, L.D., Palmer, J.G., DJMS, Bowman, 2019. Two climate sensitive tree-ring chronologies from Arnhem land, monsoonal Australia. *Austral Ecol.* 44, 581–596.
- Ashok, K., Behera, S.K., Rao, S.A., Weng, H., Yamagata, T., 2007. El Niño Modoki and its possible teleconnection. *J. Geophys. Res.* 112, C11007 <https://doi.org/10.1029/2006JC003798>.
- Baker, P.J., Palmer, J.G., D'Arrigo, R., 2008. The dendrochronology of *Callitris intratropica* in northern Australia: annual ring structure, chronology development and climate correlations. *Aust. J. Bot.* 56, 311–320.
- Becker, A., Finger, P., Meyer-Christoffer, A., Rudolf, B., Schamm, K., Schneider, U., Ziese, M., 2013. A description of the global land-surface precipitation data products of the Global Precipitation Climatology Centre with sample applications including centennial (trend) analysis from 1901–present. *Earth Sys. Sci. Data* 5, 71–99. <https://doi.org/10.5194/esd-5-71-2013>.
- Brown, J.R., Moise, A.F., Colman, R., Climate, H.Z.J.O., 2016. Will a warmer world mean a wetter or drier Australian monsoon? *J. Atmos. Sci.* <https://doi.org/10.1175/JCLI-D-15-0695.s1>.
- Buckley, B.M., Anchukaitis, K.J., Penny, D., Fletcher, D., Cook, E.R., Sano, M., Nam, L.C., Wichienkeeo, A., Minh, T.T., Hong, T.M., 2010. Climate as a contributing factor in the desire of Angkor, Cambodia. *Proc. Natl. Acad. Sci.* 107, 6748–6752.
- Cai, W., Cowan, T., 2009. La Niña Modoki impacts Australian autumn rainfall variability. *Geophys. Res. Lett.* 36, L12805 <https://doi.org/10.1029/2009GL037885>.
- Cook, B., 2019. Drought: An Interdisciplinary Perspective. Columbia University Press, New York (215pp).
- Cook, G.D., Heerdegen, R.G., 2001. Spatial variation in the duration of the rainy season in monsoonal Australia. *Int. J. Climatol.* 21, 1723–1732.
- Cook, E.R., Meko, D.M., Stahle, D.W., Cleaveland, M.K., 1999. Drought reconstructions for the continental United States. *J. Clim.* 12, 1145–1162.
- Cook, E.R., Anchukaitis, K.J., Buckley, B.M., D'Arrigo, R.D., Jacoby, G.C., Wright, W.E., 2010. Asian monsoon failure and megadrought during the last millennium. *Science* 328, 486–489.
- D'Arrigo, R., Abram, N., Ummenofer, C., Palmer, J., Mudelsee, M., 2011. Reconstructed streamflow for Citarum River, Java. *Clim. Dyn.* 36, 451–462.
- Drosdowsky, W., 1996. Variability of the Australian summer monsoon at Darwin: 1957–1992. *J. Clim.* 9, 85–96.
- Evans, S., Marchand, R., Ackerman, T., 2014. Variability of the Australian monsoon and precipitation trends at Darwin. *J. Clim.* 27, 8488–8500.
- Freund, M.B., Henley, B.J., Karoly, D.J., McGregor, H.V., Abram, N.J., Dommenget, D., 2019. Higher frequency of Central Pacific El Niño events in recent decades relative to past centuries. *Nat. Geosci.* <https://doi.org/10.1038/s41561-019-0353-3>.
- Fritts, H.C., 1976. Tree Rings and Climate. Academic Press, New York (567pp).
- Gallant, A.J.E., Reeder, M.J., Risbey, J.S., Hennessy, K.J., 2013. The characteristics of seasonal-scale droughts in Australia, 1911–2009. *Int. J. Climatol.* 33, 1658–1672.
- Ghelani, R.P.S., Oliver, E.C.M., Holbrook, N.J., Wheeler, M.C., Klotzbach, P.J., 2017. Joint modulation of intraseasonal rainfall in tropical Australia by the Madden-Julian Oscillation and El Niño Southern Oscillation. *Geophys. Res. Lett.* <https://doi.org/10.1002/2017GL075452>.
- Godfree, R.C., Knerr, N., Godfree, D., Busby, J., Robertson, B., Encias-Viso, F., 2019. Historical reconstruction unveils the risk of mass mortality and ecosystem collapse during pancontinental megadrought. *Proc. Natl. Acad. Sci.* <https://doi.org/10.1073/pnas.1902046116>.
- Goswami, B.N., Venugopal, V., Chattopadhyay, R., 2019. South asian monsoon extremes. Ch 2. In: Venugopal, V., Sukhatme, J., Murtugudde, R., Roca, R. (Eds.), Tropical Extremes: Natural Variability and Trends. Elsevier, Netherlands (322pp).
- Hendon, H., Liebman, B., 1990. A composite study of the onset of the Australian monsoon. *J. Atmos. Sci.* 47, 2227–2240.
- Hendon, H.H., Lim, E., Wand, G., Alves, O., Hudson, D., 2009. Prospects for predicting the two flavours of El Niño. *Geophys. Res. Lett.* 36, L19713 <https://doi.org/10.1029/2009GL040100>.
- IPCC, 2019. Special report on oceans and cryosphere. Ch 6. In: Extremes, Abrupt Changes and Managing Risks (94pp).
- Kajikawa, Y., Wang, B., Yang, J., 2010. A multi-time scale Australian monsoon index. *Int. J. Climatol.* 30, 1114–1120.
- Kelley, C.P., Mohtadi, S., Cane, M.A., Seager, R., Kushnir, Y., 2015. Climate change in the Fertile Crescent and implications of the recent Syrian drought. *Proc. Natl. Acad. Sci.* 112, 3241–3246.
- King, A.D., Alexander, L.V., Donat, M.G., 2013. Asymmetry in the response of eastern Australia extreme rainfall to low-frequency Pacific variability. *Geophys. Res. Lett.* 40 (10), 2271–2277. <https://doi.org/10.1002/grl.50427>.
- Kug, J.-S., Ham, Y.-G., 2011. Are there two types of La Niña? *Geophys. Res. Lett.* 38, L16704 <https://doi.org/10.1029/2011GL048237>.
- Kug, J.-S., An, S.-I., Jin, F.-F., 2009. Two types of El Niño events: cold tongue El Niño and warm pool El Niño. *J. Clim.* 22, 1499–1515.
- Larkin, N., Harrison, D.E., 2005. On the definition of El Niño and associated average U.S. weather anomalies. *Geophys. Res. Lett.* 32, L13705 <https://doi.org/10.1029/2005GL022738>.
- Lesk, C., Rowhani, P., Ramankutty, N., 2016. Influence of extreme weather disasters on global crop production. *Nature* 529 (7584), 84–87.
- Li, J., Xie, S.-P., Cook, E.R., Morales, M.S., Christie, D.A., Johnson, N.C., Chen, F., D'Arrigo, R., Fowler, M., Gou, X., Fang, K., 2013. El Niño modulation over the past seven centuries. *Nat. Clim. Chang.* <https://doi.org/10.1038/NCLIMATE1936>.
- Liebman, B., Smith, C.A., 1996. Description of a complete interpolated outgoing longwave radiation dataset. *Am. Meteorol. Soc.* 77 (6), 1275–1277.
- McBride, J.L., Nicholls, N., 1983. Seasonal relationships between Australian rainfall and the Southern Oscillation. *Mon. Weather Rev.* 111, 1998–2004.
- Melvin, T.M., Briffa, K.R., 2008. A “signal-free” approach to dendroclimatic standardisation. *Dendrochronologia* 26, 71–86.
- Meyers, G., McIntosh, P., Pigot, L., Pook, M., 2007. The years of El Niño, La Niña and interactions with the tropical ocean. *J. Clim.* 20, 2872–2880.
- Moise, A., et al., 2015. Monsoonal north cluster report. In: Ekstrom, M., et al. (Eds.), Climate Change in Australia Projections for Australia's Natural Resource Management Regions: Cluster Reports. CSIRO and Bureau of Meteorology, Australia.
- Nicholls, N., McBride, J.L., Omerod, R.J., 1982. On predicting the onset of the Australian wet season at Darwin. *Mon. Weather Rev.* 109, 2435–2443.
- O'Donnell, A.J., Cook, E.R., Palmer, J.G., Turney, C.S.M., Grierson, P.F., 2018. Potential for tree rings to reveal spatial patterns of past drought variability across western Australia. *Environ. Res. Lett.* 13, 024020.
- Palmer, J.G., Cook, E.R., Turney, C.S.M., Allen, K., Fenwick, P., Cook, B.I., O'Donnell, A., Lough, J., Grierson, P., Baker, P., 2015. Drought variability in the eastern Australia and New Zealand summer drought atlas (ANZDA, CE 1500–2012) modulated by the Interdecadal Pacific Oscillation. *Environ. Res. Lett.* 10, 1–12, 124002.
- Pederson, N., Hessl, A.E., Baatarbileg, N., Anchukaitis, K.J., Di Cosmo, N., 2014. Pluvials, droughts, the Mongol Empire and modern Mongolia. *Proc. Natl. Acad. Sci.* 111, 4375–4379.
- Power, S., Haylock, M., Colman, R., Wang, X., 2006. The predictability of interdecadal changes in ENSO activity and ENSO teleconnections. *J. Clim.* 19 (19), 4755–4771.
- Rayner, N.A., Parker, D.E., Horton, E.B., 2003. Global analyses of sea surface temperature, sea ice, and night marine air temperature since the late nineteenth century. *J. Geophys. Res.* 108 (D14), 4407. <https://doi.org/10.1029/2002JD002670/full>.
- Redhead, T.D., 1979. On the demography of *Rattus sordidus colletti* in monsoonal Australia. *Aust. J. Ecol.* 4, 115–136.
- Rensch, P., 2019. Mechanisms causing east Australian spring rainfall differences between three strong El Niño events. *Clim. Dyn.* <https://doi.org/10.1007/s00382-019-04732-1>.

- Risbey, J.S., Pook, M.J., McIntosh, P., 2009. On the remote drivers of rainfall variability in Australia. *Mon. Weather Rev.* 137 (10), 3233–3253. <https://doi.org/10.1175/2009MWR2861.1>.
- Rojas, R., Feyen, L., Watkiss, P., 2013. Climate change and river floods in the European Union: socio-economic consequences and costs and benefits of adaptation. *Glob. Environ. Chang.* 23 (6), 1737–1751.
- Smerdon, J.E., PAGES Hydro 2k consortium, 2017. Comparing proxy and model estimates of hydroclimate variability and change over the Common Era. *Clim. Past* 13, 1851–1900.
- Song, L., Chen, S., Chen, W., Chen, X., 2017. Distinct impacts of two types of La Niña events on Australian summer rainfall. *Int. J. Climatol.* 37, 2532–2544.
- Taschetto, A.S., England, M.H., 2009. El Niño Modoki impacts on Australian rainfall. *J. Clim.* 22, 3167–3174.
- Taschetto, A.S., Ummenhofer, C.C., Gupta Sen, A., England, M.H., 2009. Effect of anomalous warming in the Central Pacific on the Australian monsoon. *Geophys. Res. Lett.* 36 (12), C11007–5 <https://doi.org/10.1029/2009GL038416>.
- Taylor, J.A., Tulloch, D., 1985. Rainfall in the wet-dry tropics: extreme events at Darwin and similarities between years during the period 1870–1983 inclusive. *Aust. J. Ecol.* 10, 281–295.
- Vardon, M.J., Brocklehurst, P.S., Woinarski, J.C.Z., Cunningham, R.B., Donnelly, C.F., Tiderman, C.R., 2001. Seasonal habitat use of flying-foxes, *Pteropus alecto* and *P. scapilatus* (Megachiroptera), in monsoonal Australia. *J. Zool. Soc. London* 253, 523–535.
- Vicente-Serrano, S.M., Beguería, S., López-Moreno, J.I., Angulo, M., El Kenawy, A., 2010. A global 0.5° gridded dataset (1901–2006) of a multiscalar drought index considering the joint effects of precipitation and temperature. *J. Hydrometeorol.* 11 (4), 1033–1043.
- Wang, G., Hendon, H.H., 2007. Sensitivity of Australian rainfall to inter-El Niño variations. *J. Clim.* 20, 4211–4226.
- Warfe, D.M., Pettit, N.E., Davies, P.M., Pusey, B.J., Hamilton, S.K., Kennard, M.J., Townsend, S.A., Bayliss, P., Ward, D.P., Douglas, M.M., Burford, M.A., Finn, M., Bunn, S.E., Halliday, I.A., 2011. The “wet-dry” in the wet-dry tropics drives river ecosystem structure and processes in northern Australia. *Freshw. Biol.* 56 (11), 2169–2195. <https://doi.org/10.1111/j.1365-2427.2011.02660.x>.
- Williams, I.N., Patricola, C.M., 2018. Diversity of ENSO events unified by convective threshold sea surface temperatures: a nonlinear ENSO index. *Geophys. Res. Lett.* 45, 9236–9244.
- Woinarski, J., Mackey, B., Nix, H., Traill, B., 2007. The Nature of Northern Australia ANU E-Press. Australia, Canberra, 125pp.
- Yeates, S.J., Abrecht, D.G., Price, T.P., Mollah, W.S., Hausrler, P., 1996. Operational aspects of ley farming systems in the semi-arid tropics of northern Australia: a review. *Aust. J. Exp. Agric.* 36 (8), 1025–1035. <https://doi.org/10.1071/EA9961025>.
- Zhang, W., Li, H., Jin, F.-F., Stuecker, M.F., Turner, A.G., Klingaman, N.P., 2015. The annual-cycle modulation of meridional asymmetry in ENSO's atmospheric response and its dependence on ENSO zonal structure. *J. Clim.* 28 (14), 5795–5812. <https://doi.org/10.1175/JCLI-D-14-00724.1>.
- Zhang, T., Yang, S., Jiang, X., Zhao, P., 2016. Seasonal-interannual variation and prediction of wet and dry season rainfall over the Maritime Continent: roles of ENSO and monsoon circulation. *J. Clim.* 29, 3675–3695.